International Journal of Hydrogen Energy 238 (2026) 155412

Contents lists available at ScienceDirect

International Journal of Hydrogen Energy

journal homepage: www.elsevier.com/locate/he

Adaptive neural network controller for CA50 optimization under multiple constraints in hydrogen internal combustion engines

Pier Paolo Brancaleoni, Enrico Corti *, Alessandro Rossi, Vittorio Ravaglioli, Alessandro Brusa, Nicolò Cavina

DIN – Dipartimento di Ingegneria Industriale, Alma Mater Studiorum – Università di Bologna, Bologna, 40121, Italy

ARTICLE INFO

Keywords:
Combustion control
Artificial neural network
Adaptive control
Engine reliability
Hydrogen internal combustion engine

ABSTRACT

Hydrogen-fuelled internal combustion engines are a promising solution for sustainable mobility, but their efficiency strongly depends on combustion phasing, commonly quantified by the crank angle at 50% mass fraction burned (CA50). This work presents an adaptive CA50 controller that maximizes efficiency while maintaining reliability with respect to knock intensity and peak cylinder pressure (Pmax). Artificial neural networks (ANNs) are used to model the dependence of brake thermal efficiency, Pmax and knock intensity on CA50. To ensure robust performance under varying or aged conditions, ANN parameters are continuously updated online using real-time combustion data. The updated ANN outputs are processed through a desirability function to determine the optimal CA50 target. Simulation results show improved efficiency under off-design conditions: a 5% increase in EGR is compensated by advancing CA50 by about 4°, recovering most of the baseline efficiency while respecting Pmax and knock constraints. Real-time feasibility was confirmed on embedded hardware.

SYMBOLS/ABBREVIATIONS

AML	Adaptive Machine Learning
ANN	Artificial Neural Network
BEV	Battery-Electric Vehicle
BMEP	Brake Mean Effective Pressure
BSFC	Brake Specific Fuel Consumption
BTE	Brake Thermal Efficiency
CA50	Crank Angle where 50 % of the Energy is Released
cRIO	Compact Reconfigurable Input/Output
D	Desirability Function
$\mathbf{d_{BTE}}$	BTE's desirability function
$\mathbf{d_k}$	Single desirability function
$\mathbf{d_{MAPO}}$	MAPO's desirability function
$\mathbf{d_{Pmax}}$	Pmax's desirability function
E	Error
EGR	Exhaust Gas Recirculation
f	Trend of considered function
FMEP	Friction Mean Effective Pressure
GDM	Gradient Descent with Momentum
$\mathbf{H_2ICE}$	Hydrogen Internal Combustion Engine
IMEP	Indicated Mean Effective Pressure
LHV	Lower Heating Value
$\mathbf{Lower_{BTE}}$	Lower Limit BTE
$\mathbf{Lower_{MAPO}}$	Lower Limit MAPO
$\mathbf{Lower_{Pmax}}$	Lower Limit Pmax
LuT	Look-up Table
$\mathbf{m_{fuel}}$	Injected fuel mass
OP	Operating Point
PFI	Port Fuel Injection
Pmax	Peak Cylinder Pressure
$\mathbf{r_k}$	Desirability function weight
SA	Spark Advance
$\mathbf{Upper_{BTE}}$	Upper Limit BTE
$\mathbf{Upper_{MAPO}}$	Upper Limit MAPO
$\mathbf{Upper_{Pmax}}$	Upper Limit Pmax
v	Parameter for GDM explanation
$\mathbf{V_d}$	Cylinder displacement
VGT	Variable Geometry Turbine
w	ANN weights
$\mathbf{w_t}$	Desirability function shape factor
η	Learning Rate
λ	Air-to-hydrogen normalized ratio
μ	Momentum Coefficient

* Corresponding author.
E-mail addresses: pier.brancaleoni2@unibo.it (P.P. Brancaleoni), enrico.corti2@unibo.it (E. Corti), rossialessandro1508@gmail.com (A. Rossi), vittorio.ravaglioli2@unibo.it (V. Ravaglioli), alessandro.brusa6@unibo.it (A. Brusa), nicolo.cavina@unibo.it (N. Cavina).

https://doi.org/10.1016/j.ijhydene.2026.155412
Received 3 November 2025; Received in revised form 1 April 2026; Accepted 4 May 2026
Available online 7 May 2026

1. Introduction

The ongoing global effort to decarbonize the transportation sector is driving the rapid development and deployment of alternative powertrain technologies that can meet stringent environmental regulations while maintaining or even enhancing vehicle performance and reliability. Among these technologies, Hydrogen Internal Combustion Engines (H_2ICEs) represent a compelling solution, combining the well-understood mechanical architecture of conventional engines with the carbon-free combustion properties of hydrogen fuel [1]. When produced from renewable energy sources, hydrogen offers a sustainable energy vector with the potential to significantly reduce the lifecycle greenhouse gas emissions associated with transportation [2]. Unlike Battery-Electric Vehicles (BEVs), which rely on critical raw materials and still face challenges related to energy density, charging infrastructure, and sustainability of battery production, H_2ICEs offer the advantage of fast refuelling, high energy density, and compatibility with existing manufacturing and maintenance ecosystems [1,3,4]. These factors position H_2ICEs as a particularly attractive option for sectors where operational flexibility and range are paramount and decarbonization is required [5,6]. Despite these advantages, the widespread adoption of H_2ICEs is still hindered by several technical limitations [7,8]. Hydrogen combustion exhibits unique characteristics (including high flame speed, wide flammability limits, and low ignition energy) that differentiate it from conventional hydrocarbon fuels [1,9]. While these properties can lead to high thermal efficiency and ultra-lean operation, they also introduce complex challenges such as increased susceptibility to knock, pre-ignition, backfiring (for Port Fuel Injection, PFI), and high NOx emissions under certain conditions [9–12]. Moreover, operating with extremely lean mixtures and retarded combustion phasing to mitigate NOx emissions and knocking often causes significant efficiency losses [11,13]. This drawback, combined with the need to achieve high Brake Mean Effective Pressures (BMEPs), leads to use high boost pressures, which can result in excessive peak firing pressures (Pmax) and consequently require further combustion retardation [14]. These trade-offs highlight the need for innovative engine control strategies capable of optimizing combustion in real time, balancing performance, efficiency, and emissions [15]. Moreover, H_2ICEs are generally equipped with Exhaust Gas Recirculation (EGR) circuits to reduce peak temperatures, thus NOx emissions and knocking risk [11,16–18]. However, these systems typically do not use direct feedback control. As a result, any fluctuation, instability or malfunctioning in EGR delivery can lead the engine to operate under suboptimal conditions, compromising both efficiency, reliability and emissions.

To address these challenges, adaptive control strategies are emerging as a powerful solution thanks to their capability to adapt under evolving environment and conditions [19–24]. By continuously updating control parameters based on feedback from the engine and external sensors, adaptive algorithms can respond to changing conditions such as ambient temperature, engine wear, or component's malfunctioning.

In the last years, the use of machine learning techniques has also gained momentum in the domain of internal combustion engine modelling and control, where they are proving effective in representing nonlinear behaviours [15,25–32]. These techniques may be used with different objectives.

- offline modelling and prediction [15,25–32], where ANNs capability to capture nonlinear multi-variable relationships is used to setup black-box models;
- online/real-time non-adaptive control [31,32], where the ANNs are used for soft sensing and diagnosis. ANNs are trained off-line and are used in real-time to replace complex models.

The adoption of Artificial Neural Networks (ANNs) has been proven particularly interesting in capturing the nonlinear, multi-variable relationships characteristic of combustion phenomena as for the correlation between Spark Advance (SA) position and relative Crank Angle where 50 % of the Energy is Released (CA50) under different operating conditions (i.e., air-to-fuel mixture quality, engine speed, EGR rate, etc.) [15,25,32].

Overall, recent comprehensive reviews [31,32] highlight that artificial neural networks are predominantly applied as off-line prediction tools or surrogate models for engine calibration and optimization. Despite their recognized potential, ANN-based combustion control strategies operating in real time remain tied to an off-line calibration process, which prevents the capability of adapting to actual conditions. In Ref. [32] the authors point out that ANN are black-box models trained on limited database, thus their reliability is limited to the training domain. Static ANNs which only rely on offline training will not be robust with respect to EGR or AFR variations with respect to nominal conditions.

On the other hand, recently, the integration of machine learning techniques in adaptive controls is gaining traction in different fields of application [33–36]: in Ref. [33] the authors systematically compare Adaptive Machine Learning (AML) with Static Machine Learning (SML) techniques, concluding that AML should be used when controlled systems are time-varying, or tend to drift. The robustness of AML to drift, yet observed on a different plant (particle accelerators), is confirmed in Ref. [34]. Wu et al. in Ref. [35] show how AML can be actually implemented in the feedback control loop of chemical processes. Wong et al. in Ref. [36] show that an adaptive neural network can be successfully implemented within the engine idle controller, but AML has never been applied to control the combustion process, with the aim of a continuous optimization.

Previous studies, including [15], have shown that CA50 is a physically meaningful control variable to optimize the combustion process, owing to its strong correlation with combustion phasing, torque generation, and efficiency. In such approaches, CA50 is typically regulated around a predefined target to achieve a desired engine output. However, under varying operating conditions, the optimal CA50 value itself may shift, motivating the need for adaptive strategies capable of identifying the optimal CA50 target in real time rather than enforcing a fixed reference.

Although artificial neural networks have been widely adopted for engine modelling and control, the majority of existing studies are limited to off-line trained or static neural architectures, whose performance degrades under off-design conditions and time-varying phenomena such as EGR rate variations. Recent adaptive neural control approaches mainly address tracking and disturbance rejection problems and do not explicitly tackle the online optimization of combustion phasing. In this context, the present study fills an open research gap by introducing an adaptive ANN-based control strategy capable of continuously updating the CA50–performance relationships in real time and computing an optimal combustion phasing target under reliability constraints, without requiring offline re-calibration.

The proposed approach is evaluated under various operating conditions, demonstrating its effectiveness in maximizing combustion efficiency while addressing the reliability limits. Owing to its adaptive capabilities, the proposed methodology can dynamically identify and adjust the optimal CA50, compensating for disturbances such as drifting EGR actuation, or increased engine's knock tendency resulting from system aging or component degradation.

2. Materials and methods

2.1. Engine model and baseline control strategy

The activity has been carried out on a previously developed virtual H_2ICE platform [15,37] referring to a 6 cylinder double PFI spark-ignition hydrogen-fuelled engine equipped with a high-pressure EGR loop. To avoid the need for extensive test bench testing, the model was developed and validated within a software-in-the-loop

framework [38], allowing for virtual calibration and performance assessment under a wide range of operating conditions without the risk of compromising the engine under calibration phase. The engine model is capable to represent with good accuracy the main indicated combustion metrics, such as CA50, Indicated Mean Effective Pressure (IMEP), Pmax, knock intensity (quantified by means of Maximum Amplitude of Pressure Oscillations, MAPO), as a function of control parameters (i.e., throttle position, injected fuel mass, SA timing, etc.) and engine speed. Moreover, an innovative CA50-based control strategy (Fig. 1, partially derived from Ref. [15]) has been developed and validated based on the same engine model, allowing to achieve the desired CA50 under steady and transient conditions, enabling greater engine management flexibility.

Considering Fig. 1, the optimal CA50 is selected based either on Look-up Tables (LuTs) as a function of engine speed, load and air-to-hydrogen normalized ratio (λ), as reported in Ref. [15] (however, this approach does not allow to adjust the CA50 under system evolution nor component's malfunctioning, due to the use of 'permanent' LuTs determining the CA50 optimal setting), or can be dynamically selected based on system's evolution. Further corrections to CA50 are then applied to enable fast torque management: the CA50 setting is retarded under fast negative demanded torque gradient to achieve the requested target when torque cannot be further decreased acting on the injected fuel mass, due to lower saturation, to avoid misfire [15]. The CA50 degradation and limitation blocks represent supervisory logic based on real-time combustion indicators, using look-up tables or ANNs rather than explicit physical models, and are used to constrain the CA50 optimization domain under off-design conditions.

Focusing on the second approach (the use of an adaptive algorithm), it dynamically adapts to the actual running conditions, based on the combustion metrics data flow, which was already used by the previous controller architecture for CA50, Pmax and MAPO feedback control. The further step developed in the present work is then to use the same information gathered from cylinder pressure signals to adjust the optimal combustion phasing target. The target CA50 is then converted into a corresponding SA actuation by means of a proper ANN. The CA50 feedback control (carried out by means of a PID) cancels out potential inaccuracies in the ANN converting CA50 to SA.

2.2. Adaptive control structure

In the present work, CA50 is not treated as a fixed reference to be tracked, but as a decision variable whose optimal value is continuously updated based on estimated performance trends and reliability constraints.

The adaptive control algorithm must be capable of identifying the optimal CA50 setting, considering both maximum achievable Brake Thermal Efficiency (BTE) and mechanical constraints such as Pmax and MAPO limits. Concerning BTE, even if not directly determined by means of cylinder pressure information, it can be easily estimated starting from IMEP, determining BMEP from Friction Mean Effective Pressure (FMEP), by means of a friction model, and finally using the information of the injected fuel mass, as shown in Eq. (1) and Eq. (2) [39].

$$\boldsymbol{BMEP = IMEP - FMEP} \tag{1}$$

$$\boldsymbol{BTE = \frac{BMEP \cdot V_d}{m_{fuel} \cdot LHV}} \tag{2}$$

The friction model used to estimate FMEP in equation (1) is based on the Chen-Flynn [40] approach, as shown in Ref. [15]. BTE can then be determined (Eq. (2)), multiplying BMEP by the cylinder displacement (V_d) to achieve the effective work per engine cycle, and finally dividing by the product of the injected fuel mass (m_{fuel}) by the Lower Heating Value (LHV) of the fuel.

The dynamic determination of the optimal CA50 should be computationally efficient, to enable real-time execution, due to limited processing capabilities on embedded control units.

To enable adaptive learning and real-time correction of the optimal CA50 target, a customized neural network training routine has been developed: for each considered cylinder, three neural networks are used to trace the dependence of the performance metrics BTE, Pmax and MAPO as a function of CA50. The following step consists in the definition of a desirability function, based on BTE, MAPO and Pmax to identify the optimal CA50 given reliability constraints: the influence of CA50 on the desirability function value can then be easily determined, leading to the evaluation of the optimal CA50 setting (i.e., the one maximizing the desirability function).

Each network structure consists of a single-input (CA50), single-output (performance metric: either BTE, Pmax or MAPO) feedforward fully-connected neural network with one hidden layer comprising three neurons. This simple, yet effective architecture, has been selected to ensure low computational complexity and compatibility with real-time embedded applications.

A first off-line training of the ANNs has been carried out for each one of the Operating Points (OP) representing the engine working domain: OPs are defined as the combination of engine speed, load and λ. For a given OP, the training is executed maintaining the engine model in steady-state baseline conditions (i.e., fixing engine speed, m_{fuel}, SA, EGR valve position and manifold pressure), and the corresponding ANNs' hyperparameters (biases and gains) resulting from the training are then stored in proper LuTs. Given the structure of the ANNs (three neurons), 14 LuTs are required for each performance metric, for each cylinder.

When the controller is in use, once the OP is recognized, the hyperparameters of the ANNs are extracted from the corresponding LuTs, delivering the trends of BTE, Pmax, MAPO as a function of CA50.

The described architecture would suffer of the same problem arising from the definition of optimal CA50 directly based on LuTs, (i.e., optimal phasing would not be dynamically adjusted to actual engine conditions): in fact, since the LuTs training has been carried out in baseline conditions, their output corresponding to the actual OP will not

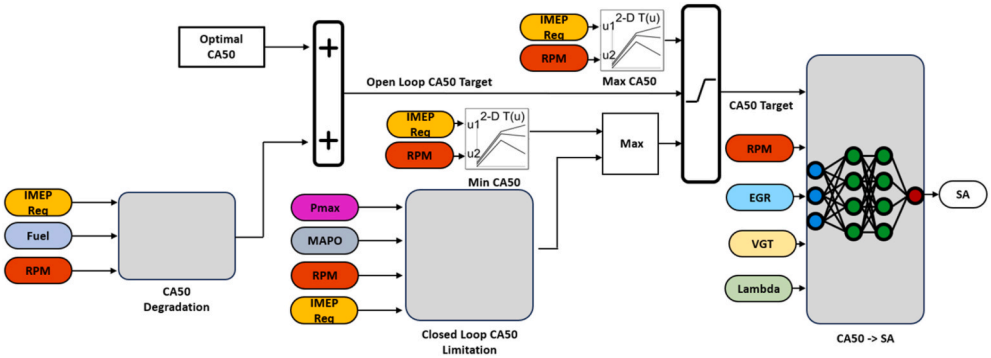

Fig. 1. CA50-based control strategy.

be valid under different engine states differing from the baseline.

To enable adaptive capabilities, an algorithm adjusting the ANNs biases and gains to actual conditions has been implemented, leveraging Gradient Descent with Momentum (GDM) [41]. The learning rate (η) and the momentum coefficient (μ) have been properly calibrated to guarantee stability while avoiding slow learning, considering that the GDM can be described as in Eq. (3), where E is the error and *w* the weights matrix.

$$\boldsymbol{v}^{(t+1)} = \boldsymbol{\mu} \cdot \boldsymbol{v}^{t} - \boldsymbol{\eta} \cdot \nabla \boldsymbol{E}(\boldsymbol{w}^{(t)}) \tag{3}$$

Therefore, the updated weight can be calculated as in Eq. (4).

$$\boldsymbol{w}^{(t+1)} = \boldsymbol{w}^{t} + \boldsymbol{v}^{(t+1)} \tag{4}$$

Fig. 2 represents the algorithm for the adaptive procedure. The adaptation of the ANNs' hyperparameters to actual conditions requires to re-train online the ANNs using the combustion metrics data flow coming from a combustion analyser. To allow a computational efficient and robust real-time training, the dataflow is mean averaged and clustered, organizing BTE, Pmax, and MAPO measurements into discrete CA50 clusters. Only once a predefined threshold of data samples is reached for a set of CA50 values in the cluster for a given OP (meaning that for each parameters at least five CA50-performance metric couples are clustered), the metrics trend is considered valid and representative of the working condition and can be used for the on-line adaptive training. The adaptive algorithm is executed with an unitary epoch each time at least one point of the performance metric considered evolves from the previous configuration (at least after 5 cycles as the output of the mean averaged performance metrics is updated each 5 cycles).

Then, the output of each updated ANN is calculated over a set of CA50 input values (query CA50 vector), delivering the corresponding BTE, Pmax and MAPO trends against CA50 (*Trends vs CA50* in Fig. 2). These trends are updated after each on-line retraining of the ANNs, which is performed every five engine cycles per cylinder. Finally, the optimal CA50 is calculated by means of a properly calibrated Desirability function (D): the formulation is selected for its computational simplicity and suitability for real-time constrained optimization, rather than for detailed combustion interpretation. As reported in Eq. (5), the Desirability function is defined based on the factors d_k and r_k, which determine the influence of the k-th combustion metric (either BTE, MAPO or Pmax) on the overall trend of D against CA50. The optimal CA50 setting delivers the highest possible value of D: this is achieved by maximizing the BTE, while introducing handicaps on CA50 settings that would lead to excessive Pmax and/or MAPO values.

$$\boldsymbol{D} = \left(\prod \boldsymbol{d}_{\boldsymbol{k}}^{\boldsymbol{r}_{\boldsymbol{k}}}\right)^{\frac{1}{\sum r_k}} \tag{5}$$

The single desirability functions of respectively BTE (d_{BTE}), Pmax (d_{Pmax}) and MAPO (d_{MAPO}) are expressed as reported in Eq. (6), Eq. (7) and Eq. (8), where *f* represents the trend of the considered parameter as a function of CA50, the *upper* and *lower* limits the maximum and minimum values expected for the considered parameters and w_t is the shape factor.

$$\begin{cases} \boldsymbol{d}_{\boldsymbol{BTE}} = \dfrac{[\boldsymbol{f}_{\boldsymbol{BTE}}(\boldsymbol{CA50}) - \boldsymbol{Lower}_{\boldsymbol{BTE}}]}{\boldsymbol{Upper}_{\boldsymbol{BTE}} - \boldsymbol{Lower}_{\boldsymbol{BTE}}} \\ \boldsymbol{d}_{\boldsymbol{BTE}}(\boldsymbol{d}_{\boldsymbol{BTE}} \le \boldsymbol{0}) = \boldsymbol{0} \\ \boldsymbol{d}_{\boldsymbol{BTE}}(\boldsymbol{d}_{\boldsymbol{BTE}} \ge \boldsymbol{1}) = \boldsymbol{1} \\ \boldsymbol{D}_{\boldsymbol{BTE}} = \boldsymbol{d}_{\boldsymbol{BTE}}^{\boldsymbol{wt}_{\boldsymbol{BTE}}} \end{cases} \tag{6}$$

$$\begin{cases} \boldsymbol{d}_{\boldsymbol{Pmax}} = \dfrac{[\boldsymbol{f}_{\boldsymbol{Pmax}}(\boldsymbol{CA50}) - \boldsymbol{Lower}_{\boldsymbol{Pmax}}]}{\boldsymbol{Upper}_{\boldsymbol{Pmax}} - \boldsymbol{Lower}_{\boldsymbol{Pmax}}} \\ \boldsymbol{d}_{\boldsymbol{Pmax}}(\boldsymbol{d}_{\boldsymbol{Pmax}} \le \boldsymbol{0}) = \boldsymbol{0} \\ \boldsymbol{d}_{\boldsymbol{Pmax}}(\boldsymbol{d}_{\boldsymbol{Pmax}} \ge \boldsymbol{1}) = \boldsymbol{1} \\ \boldsymbol{D}_{\boldsymbol{Pmax}} = \boldsymbol{d}_{\boldsymbol{Pmax}}^{\boldsymbol{wt}_{\boldsymbol{Pmax}}} \end{cases} \tag{7}$$

$$\begin{cases} \boldsymbol{d}_{\boldsymbol{MAPO}} = \dfrac{[\boldsymbol{f}_{\boldsymbol{MAPO}}(\boldsymbol{CA50}) - \boldsymbol{Lower}_{\boldsymbol{MAPO}}(\boldsymbol{OP})]}{\boldsymbol{Upper}_{\boldsymbol{MAPO}} - \boldsymbol{Lower}_{\boldsymbol{MAPO}}} \\ \boldsymbol{d}_{\boldsymbol{MAPO}}(\boldsymbol{d}_{\boldsymbol{MAPO}} \le \boldsymbol{0}) = \boldsymbol{0} \\ \boldsymbol{d}_{\boldsymbol{MAPO}}(\boldsymbol{d}_{\boldsymbol{MAPO}} \ge \boldsymbol{1}) = \boldsymbol{1} \\ \boldsymbol{D}_{\boldsymbol{MAPO}} = \boldsymbol{d}_{\boldsymbol{MAPO}}^{\boldsymbol{wt}_{\boldsymbol{MAPO}}} \end{cases} \tag{8}$$

It is worth pointing out that, while a fixed limit (given by engine manufacturer) can be set for Pmax [14], the threshold for MAPO should change according to the OP (e.g., engine speed) [15]. The contribution of BTE to the desirability function will obviously be monotonical: the higher the BTE, the higher the desirability. The CA50 optimizing the desirability over the query cluster is then set as the *Optimal CA50* in Fig. 1.

The controller is able to update the optimal values in real time in response to malfunctions, aging effects, or changes in hydrogen properties, and potentially enables a significant reduction in the number of tests required to calibrate optimal control settings, since it is capable of self-calibrating the optimal CA50.

3. Results and discussion

3.1. Validation under nominal conditions

In the proposed framework, CA50 is treated as a decision variable whose optimal value is continuously updated based on the reconstructed performance trends and the active reliability constraints. As operating conditions evolve, the relative trade-off between efficiency and combustion robustness changes: to assess the proposed algorithm capability of tracking the optimal combustion phase, tests should be conducted in

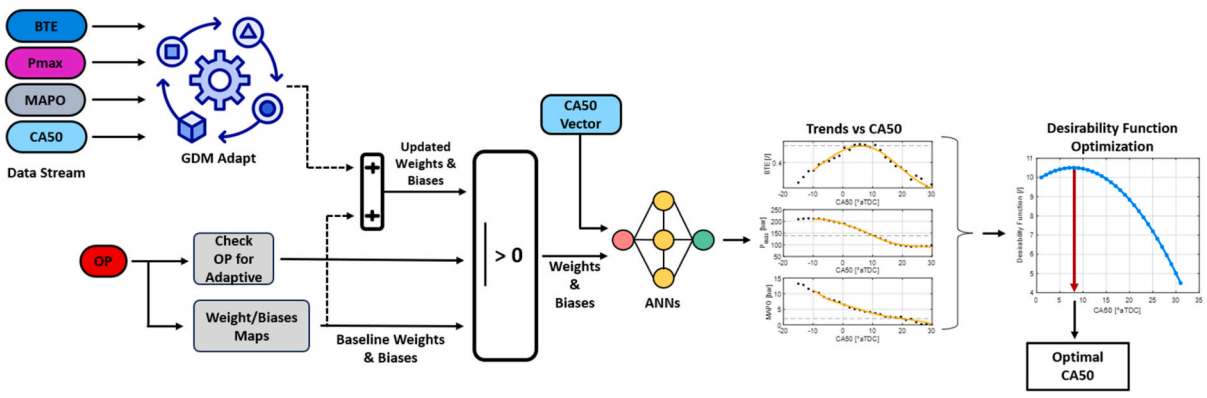

Fig. 2. Adaptive CA50 control strategy.

different scenarios.

At first, the adaptive performance of the model has been assessed under steady-state OPs. Starting from a first tentative pre-calibrated set of parameters, the algorithm has been run for a fixed amount of cycles. Fig. 3 represents an example of the results obtained in three different OPs: 1000 rpm, 5 bar of BEMP, 3000 rpm, 14 bar of BEMP and 4000 rpm, 9 bar of BEMP to cover a significant portion of the engine operating envelope [15,16]. As it can be observed, the controller averages (black dots) the cycle-by-cycle values (red dots) of each variable in the cluster of pre-defined CA50 values (from −15 °aTDC to +30 °aTDC). In the meantime, the ANNs are trained and provide the final trend of each of the three performance metrics (yellow lines). As visible, in all the considered conditions, the algorithm correctly replicates the shape of the metrics distribution over CA50 (i.e., BTE, Pmax, MAPO) as a function of CA50. Despite the modelling of the performance metrics is out of interest for negative CA50s (optimal CA50 is always positive [40]), it has been decided to feed the ANNs even with negative CA50 values to ensure robustness in the training phase (i.e., avoiding slightly positive CA50 to be close to the training boundary).

After the assessment of the capability of the system to represent the correct trends of BTE, Pmax and MAPO, the ability of the desirability function to maximize BTE while sticking to the constraints has been assessed. As visible in Fig. 4, the desirability function correctly identifies the minimum CA50 (thus *Optimal CA50*) that keeps both ANNs' Pmax and MAPO below their respective limits (black dashed lines in Fig. 4b and c).

3.2. Validation under off-design conditions

The next step is the assessment of the adaptability of the control system to conditions that may deviate from the baseline engine behaviour: the combustion controller should be able to optimize CA50 even under off-design conditions, changing the settings with respect to the baseline training. This aspect is particularly important to keep the engine working in optimal conditions without tethering engine's reliability even under aged or faulty conditions.

3.2.1. Fault EGR

The first off-design state here considered is represented by a fault in the EGR circuit: EGR rate is increased by 5%. As the recirculated exhaust gas fraction usually is not feedback controlled with proper sensors, deviations from target recirculated quantities are likely to happen, during engine's life. Since EGR is usually adopted to abate NOx formation [17], the NOx sensor can be used to identify a faulty condition of the EGR circuit, but only in cases of reduced EGR flow, and not the other way around. Other indirect estimations are possible, especially leveraging the cylinder pressure information, yet the capability of keeping the combustion phase always under control, with optimal settings is extremely useful.

Fig. 5 reports the effect of increased EGR rate on the combustion metrics trend over CA50. As it can be noticed, the higher EGR rate shows detrimental effects on BTE, while heavily reducing the MAPO distribution and shifting the engine point from being knock-constrained to peak pressure-constrained: Pmax increases while increasing EGR rate, as the intake air mass is kept constant, thus the total mass trapped in the cylinder is higher, leading to higher motoring pressure and Pmax [14]. The controller detects the system's evolution and adapts the target CA50 advancing it from 17 °aTDC to 13 °aTDC. It is worth noticing that the new working point almost reaches the same peak efficiency of the baseline configuration (by advancing CA50), while BTE would have been much lower without the adaptation of optimal combustion phasing (i.e., keeping CA50 constant despite the variation in EGR flow).

As visible from Fig. 5, the controller correctly adapts the performance metrics trends as a function of CA50, moving from the yellow characteristics to the light blue one (which match the mean points, in black, of the new operating condition, i.e., higher EGR rate). As already

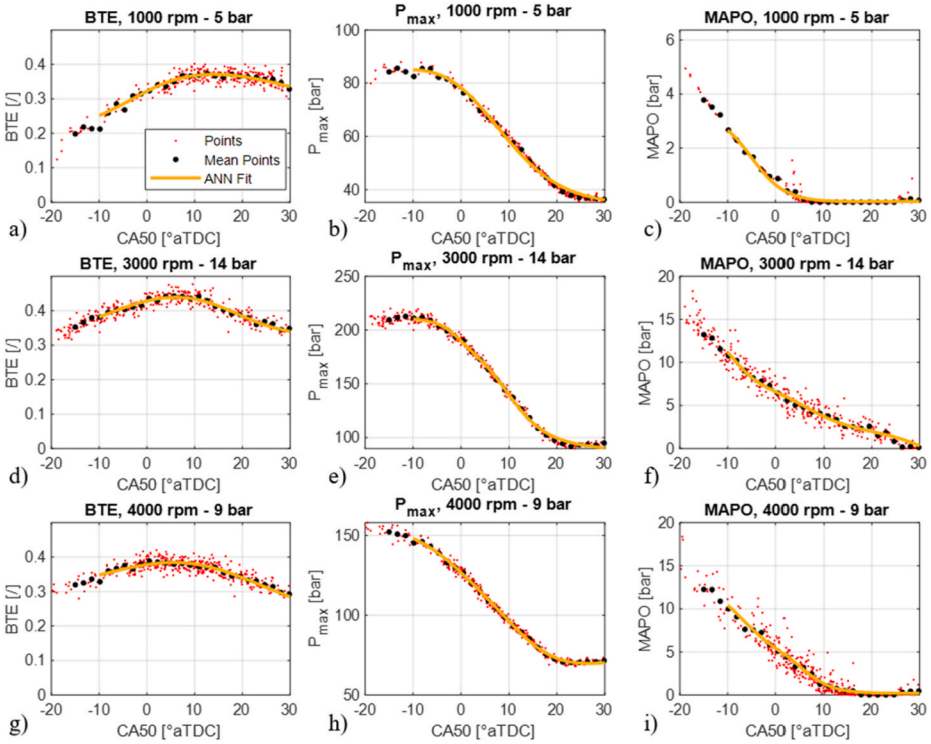

Fig. 3. BTE, Pmax and MAPO as a function of CA50 for three different operating conditions, sample points in red, learn point in black and ANN fit in yellow: a) BTE 1000 rpm - 5 bar, b) Pmax 1000 rpm - 5 bar, c) MAPO 1000 rpm - 5 bar, d) BTE 3000 rpm - 14 bar, e) Pmax 3000 rpm - 14 bar, f) MAPO 3000 rpm - 14 bar, g) BTE 4000 rpm - 9 bar, h) Pmax 4000 rpm - 9 bar and i) MAPO 4000 rpm - 9 bar. (For interpretation of the references to colour in this figure legend, the reader is referred to the Web version of this article.)

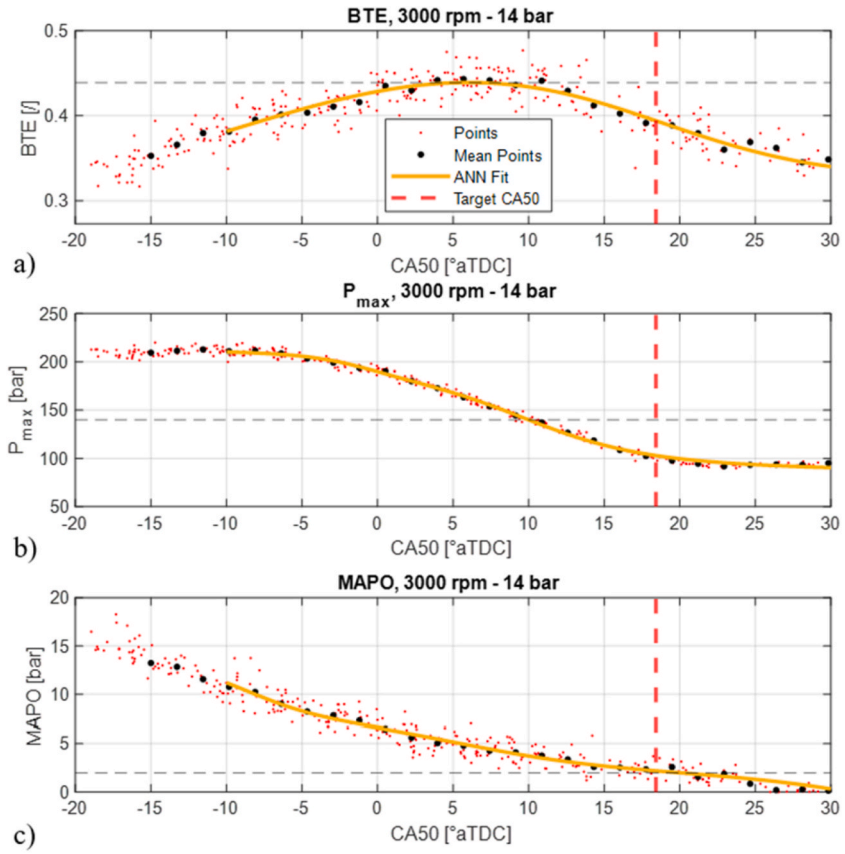

Fig. 4. BTE (a), Pmax (b) and MAPO (c) as a function of CA50 at 3000 rpm and 14 bar and identification of the target CA50 (dashed red line) that maximizes BTE while adhering to the Pmax and MAPO limits. (For interpretation of the references to colour in this figure legend, the reader is referred to the Web version of this article.)

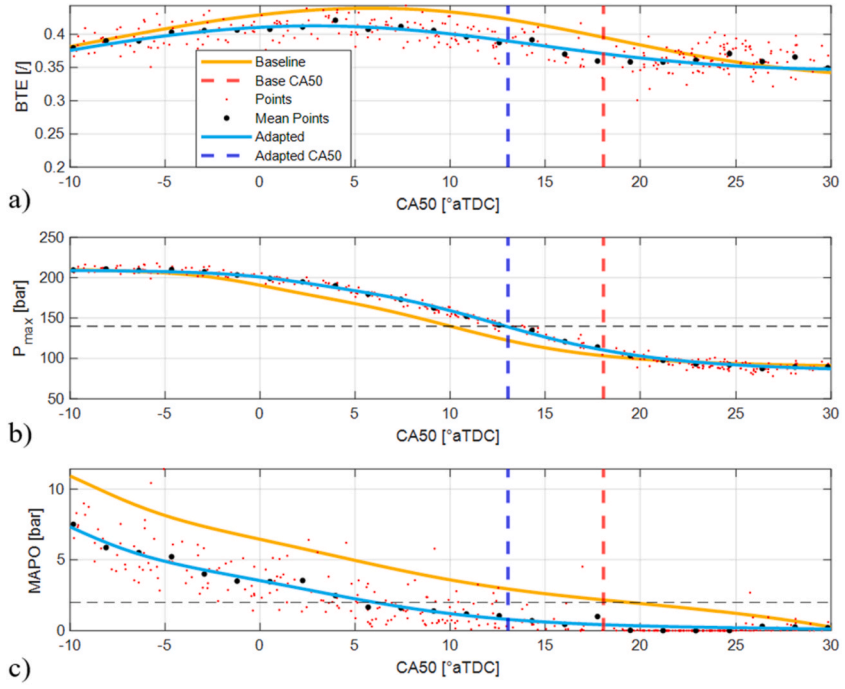

Fig. 5. BTE (a), Pmax (b) and MAPO (c) as a function of CA50, nominal traces in yellow, in light blue traces under EGR fault, blue dashed line is the nominal target CA50 and red dashed is the adapted one. (For interpretation of the references to colour in this figure legend, the reader is referred to the Web version of this article.)

recalled, the fault EGR condition leads to lower BTE, lower MAPO and higher Pmax. Therefore, the desirability function targets a more

advanced CA50 than the baseline condition. This underlines the advantage of adaptive control, avoiding to target an excessively retarded CA50 which would have reduced engine performance. In the proposed framework, these effects are not explicitly modelled, but emerge from the reconstructed performance trends.

3.2.2. Knocking condition

Another interesting condition to investigate is represented by changes in the knocking behaviour. Several causes (such as lower cooling capabilities, higher air temperature, lower humidity, etc.) [18] might lead to increased knock intensity. Even ageing might lead to higher knock intensity, due to altered lubricating capabilities, injector faults, lubricating oil retaining into combustion chamber and carbon deposits. Therefore it is interesting to assess the system's capability to properly adapt to increased knock intensity conditions. The test is carried out increasing the knock intensity evaluated by the engine model by 20%, without affecting BTE and Pmax: this hypothesis is not significant of the actual engine behaviour, but it allows assessing the controller capability to adapt to the new condition.

As reported in Fig. 6, both BTE and Pmax do not show any difference, as the only difference here is on knock sensitivity to CA50. Nonetheless, it is evident how the controller adapts to higher knock intensities, leading to a retarded optimal CA50 identified by the desirability function. In this case the operating condition is knock-limited, and the optimal CA50 is achieved where the new MAPO pattern intersects the corresponding threshold.

When knock tendency increases, the admissible CA50 range is progressively constrained by the activation of pressure- and knock-related limits. As a result, the adaptive optimization naturally converges toward more conservative CA50 values. This shift is not imposed heuristically, but results from the constrained optimization process, which excludes unsafe combustion phasing regions while still seeking the best efficiency-compatible solution.

3.2.3. Discussion

Although the proposed framework does not explicitly model combustion physics, the adaptive evolution of the CA50 target reflects well-established combustion behaviours. Under increased EGR rates, the reconstructed performance trends indicate a degradation in efficiency and combustion stability for advanced CA50 values, naturally shifting the optimal target towards later phasing. Similarly, increasing knock tendency constrains the admissible CA50 range, resulting in a conservative adjustment of the optimal combustion phasing.

These effects are not imposed a priori, but emerge from the online reconstruction of performance trends and the constrained optimization process, which together form the basis of the decision-making mechanism.

It should be noted that the controller responds to the observable effects of EGR deviation or knock tendency on combustion behaviour, without requiring explicit fault diagnosis.

3.3. Algorithm real time performance

This section presents the real-time validation of the proposed control architecture, demonstrating cycle-by-cycle execution under high-speed operating conditions.

Following the simulation phase, the proposed control algorithm has been implemented and tested on a real-time platform, to assess its capability to perform the desired calculation in actual running scenarios. The experimental setup has been based on a National Instruments 9030 Compact Reconfigurable Input/Output (cRIO) platform (with the following real time characteristics: 1.33 GHz dual core Atom, RAM 1 Gb) [42], where the Simulink model of the whole engine controller (not only the adaptive algorithm) was compiled into an executable real-time application following an Hardware-in-the-Loop approach (with real-time dataflow simulating a 4 cylinder engine was fed by a dedicated hardware unit). This allowed the algorithm to be deployed directly on the cRIO hardware for real-time testing. The implementation has been successfully validated up to 20000 rpm, demonstrating the capability of the whole control algorithm to operate under real-time constraints with a maximum execution time of 3 ms, meaning that the theoretical limit of the controller is double the reached one (being 6 ms the limit at 20000 rpm).

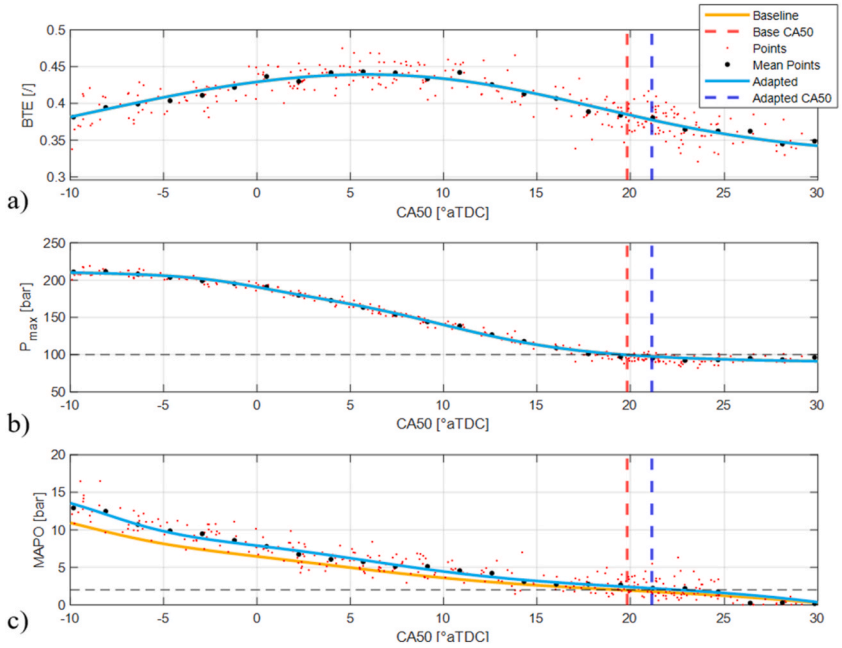

Fig. 6. BTE (a), Pmax (b) and MAPO (c) as a function of CA50, nominal traces in yellow, in light blue traces under increased knock intensity, red dashed line is the nominal target CA50 and blue dashed is the adapted one. (For interpretation of the references to colour in this figure legend, the reader is referred to the Web version of this article.)

4. Conclusions & future developments

In this study an adaptive neural network-based control for hydrogen internal combustion engines has been developed. The controller traces the trends of BTE, Pmax and MAPO as a function of CA50, using three Artificial Neural Networks (ANNs), setting the optimal CA50 thanks to a desirability function evaluated in real-time. The ANNs biases and gains are continuously updated, adapting biases and gains to fit the actual combustion metrics trend delivered by a combustion analyser. The adaptation is carried out using the *Gradient Descent with Momentum* algorithm, which proves to be compatible with real-time implementation. Thanks to this approach the combustion controller adapts the optimal CA50 to the actual conditions, maximizing engine efficiency while avoiding excessive Pmax and MAPO.

The approach has been assessed in a virtual environment, simulating a 5% variation in the EGR flow, and increasing knocking intensity by 20%: the controller is able to maximize the desirability function, quickly adapting to the present engine behaviour. The algorithm has then been implemented on a real-time embedded platform, resulting compatible with real-time execution even at extremely high engine speed.

The proposed framework combines adaptive machine learning, real-time control, and constrained combustion phasing optimization, demonstrating both methodological novelty and practical relevance. Future developments will focus on extending the framework to include NOx emissions and incorporating this aspect into the definition of the desirability function, enabling the identification of the optimal CA50 while also accounting for pollutant emissions, including those potentially evolving from cold-start conditions.

The proposed methodology represents a step toward self-calibrating combustion control strategies for hydrogen internal combustion engines, bridging the gap between adaptive machine learning and real-time engine control.

CRediT authorship contribution statement

Pier Paolo Brancaleoni: Writing – original draft, Visualization, Validation, Software, Investigation, Data curation. **Enrico Corti:** Writing – review & editing, Supervision, Project administration, Methodology, Funding acquisition, Conceptualization. **Alessandro Rossi:** Validation, Software, Data curation, Conceptualization. **Vittorio Ravaglioli:** Writing – review & editing, Funding acquisition. **Alessandro Brusa:** Writing – review & editing. **Nicolò Cavina:** Writing – review & editing.

Funding

This research has been partially funded by Ministero dell'Istruzione, dell'Università e della ricerca (MIUR) (2020R92Y3Z).

Declaration of competing interest

The authors declare the following financial interests/personal relationships which may be considered as potential competing interestsEnrico Corti, Vittorio Ravaglioli reports financial support was provided by Ministry of Education and Merit. If there are other authors, they declare that they have no known competing financial interests or personal relationships that could have appeared to influence the work reported in this paper.

References

[1] Boretti A. Hydrogen internal combustion engines to 2030. Int J Hydrog Energy Sep. 2020;45(43):23692–703. https://doi.org/10.1016/j.ijhydene.2020.06.022.
[2] Incer-Valverde J, Korayem A, Tsatsaronis G, Morosuk T. "colors" of hydrogen: definitions and carbon intensity. Energy Convers Manag Sep. 2023;291:117294. https://doi.org/10.1016/j.enconman.2023.117294.
[3] Arshad F, et al. Life cycle assessment of lithium-ion batteries: a critical review. Resour Conserv Recycl May 2022;180:106164. https://doi.org/10.1016/j.resconrec.2022.106164.
[4] Kallitsis E, Lindsay JJ, Chordia M, Wu B, Offer GJ, Edge JS. Think global act local: the dependency of global lithium-ion battery emissions on production location and material sources. J Clean Prod Apr. 2024;449:141725. https://doi.org/10.1016/j.jclepro.2024.141725.
[5] Brancaleoni PP, Damiani Ferretti AN, Corti E, Ravaglioli V, Moro D. Lifecycle CO2 analysis for urban emission reduction of hydrogen-fuelled and battery electric buses in the European Union current and future energetic scenarios. Int J Hydrog Energy Apr. 2025;123:335–53. https://doi.org/10.1016/j.ijhydene.2025.03.397.
[6] Brancaleoni P, Damiani Ferretti A, Corti E, Ravaglioli V, et al. Next-gen Italian urban mobility: emissions LCA and TCO prospective for innovative transportation solutions. SAE Int J Adv & Curr Prac in Mobility 2025;7(5):1954–67. https://doi.org/10.4271/2025-01-8593.
[7] Acar C, Dincer I. The potential role of hydrogen as a sustainable transportation fuel to combat global warming. Int J Hydrog Energy Jan. 2020;45(5):3396–406. https://doi.org/10.1016/j.ijhydene.2018.10.149.
[8] Agarwal R. Transition to a hydrogen-based economy: possibilities and challenges. Sustainability Jan. 2022;14(23). https://doi.org/10.3390/su142315975. Art. no. 23.
[9] White C, Steeper R, Lutz A. The hydrogen-fueled internal combustion engine: a technical review. Int J Hydrog Energy Aug. 2006;31(10):1292–305. https://doi.org/10.1016/j.ijhydene.2005.12.001.
[10] Li Y, Gao W, Zhang P, Fu Z, Cao X. Influence of the equivalence ratio on the knock and performance of a hydrogen direct injection internal combustion engine under different compression ratios. Int J Hydrog Energy Mar. 2021;46(21):11982–93. https://doi.org/10.1016/j.ijhydene.2021.01.031.
[11] Heffel J. NOx emission reduction in a hydrogen fueled internal combustion engine at 3000 rpm using exhaust gas recirculation. Int J Hydrog Energy Nov. 2003;28(11):1285–92. https://doi.org/10.1016/S0360-3199(02)00289-6.
[12] Khalid AH, et al. Hydrogen port fuel injection: review of fuel injection control strategies to mitigate backfire in internal combustion engine fuelled with hydrogen. Int J Hydrog Energy May 2024;66:571–81. https://doi.org/10.1016/j.ijhydene.2024.04.087.
[13] Kee S, Shioji M, Mohammadi A, Nishi M, et al. 'Knock Characteristics and Their Control with Hydrogen Injection Using a Rapid Compression/Expansion Machine'. SAE Technical Paper 2007. https://doi.org/10.4271/2007-01-1829. 2007-01-1829.
[14] Brancaleoni PP, Corti E, Silvagni G, Ravaglioli V. Physical-based peak pressure controller for hydrogen internal combustion engines. Int J Hydrog Energy Jun. 2025;133:377–85. https://doi.org/10.1016/j.ijhydene.2025.04.457.
[15] Brancaleoni PP, Corti E, Ravaglioli V, Moro D, Silvagni G. Innovative torque-based control strategy for hydrogen internal combustion engine. Int J Hydrog Energy Jul. 2024;73:203–20. https://doi.org/10.1016/j.ijhydene.2024.05.481.
[16] Arsie I, et al. A new generation of hydrogen-fueled hybrid propulsion systems for the urban mobility of the future. Energies Dec. 2023;17(1):34. https://doi.org/10.3390/en17010034.
[17] Pandey JK, Dinesh MH, Kumar GN. A comparative study of NOx mitigating techniques EGR and spark delay on combustion and NOx emission of ammonia/hydrogen and hydrogen fuelled SI engine. Energy Aug. 2023;276:127611. https://doi.org/10.1016/j.energy.2023.127611.
[18] Lai F, Sun B, Wang X, Zhang D, Luo Q, Bao L. Research on the inducing factors and characteristics of knock combustion in a DI hydrogen internal combustion engine in the process of improving performance and thermal efficiency. Int J Hydrog Energy Mar. 2023;48(20):7488–98. https://doi.org/10.1016/j.ijhydene.2022.11.091.
[19] Nesbit C, Hedrick JK. Adaptive engine control. In: 1991 American control conference; Jun. 1991. p. 2072–6. https://doi.org/10.23919/ACC.1991.4791763.
[20] Peng H, et al. A scalable, causal, adaptive rule-based energy management for fuel cell hybrid railway vehicles learned from results of dynamic programming. eTransportation May 2020;4:100057. https://doi.org/10.1016/j.etran.2020.100057.
[21] Selmanaj D, Panzani G, van Dooren S, Rosgren J, Onder C. Adaptive and unconventional strategies for engine knock control. IEEE Trans Control Syst Technol Jul. 2019;27(4):1838–45. https://doi.org/10.1109/TCST.2018.2827898.
[22] Yildiz Y, Annaswamy AM, Yanakiev D, Kolmanovsky I. Spark-ignition-engine idle speed control: an adaptive control approach. IEEE Trans Control Syst Technol Sep. 2011;19(5):990–1002. https://doi.org/10.1109/TCST.2010.2078818.
[23] Yildiz Y, Annaswamy AM, Yanakiev D, Kolmanovsky I. Spark ignition engine fuel-to-air ratio control: an adaptive control approach. Control Eng Pract Dec. 2010;18(12):1369–78. https://doi.org/10.1016/j.conengprac.2010.06.011.
[24] Tang Huajin, Weng Larry, Dong ZY, Yan Rui. Adaptive and learning control for SI engine model with uncertainties. Mechatronics, 14. IEEE/ASME Transactions on; 2009. p. 93–104. https://doi.org/10.1109/TMECH.2008.2004806.
[25] Shethia FP, Mecagni J, Brusa A, Cavina N. 'Development and Software-in-the-Loop Validation of an Artificial Neural Network-Based Engine Simulator'. presented at the Conference on Sustainable Mobility; Sep. 2022. p. 24–9. https://doi.org/10.4271/2022-24-0029.
[26] Chen C, Wu J, Wei J, Xu H. The virtual boosted DISI engine model development based on artificial neural networks. SAE technical paper 2022-01-0383. 2022. https://doi.org/10.4271/2022-01-0383.
[27] Fu J, et al. Application of artificial neural network to forecast engine performance and emissions of a spark ignition engine. Appl Therm Eng Jan. 2022;201:117749. https://doi.org/10.1016/j.applthermaleng.2021.117749.

[28] Ho T, Karri V, Lim D, Barret D. An investigation of engine performance parameters and artificial intelligent emission prediction of hydrogen powered car. Int J Hydrog Energy Jul. 2008;33(14):3837–46. https://doi.org/10.1016/j.ijhydene.2008.04.037.
[29] Jander B, Baar R. Modeling thermal engine behavior using artificial neural network. SAE Technical Paper 2017. https://doi.org/10.4271/2017-01-0534. 2017-01-0534.
[30] Tosso HG, Jardim SAB, Bloise R, Santos MMD. Spark ignition engine modeling using optimized artificial neural network. Energies Sep. 2022;15(18):6587. https://doi.org/10.3390/en15186587.
[31] Bhatt AN, Shrivastava N. Application of artificial neural network for internal combustion engines: a state of the art review. Arch Comput Methods Eng Mar. 2022;29(2):897–919. https://doi.org/10.1007/s11831-021-09596-5.
[32] Veza I, et al. Review of artificial neural networks for gasoline, diesel and homogeneous charge compression ignition engine. Alex Eng J Nov. 2022;61(11):8363–91. https://doi.org/10.1016/j.aej.2022.01.072.
[33] Gheibi O, Weyns D, Quin F. Applying machine learning in self-adaptive systems: a systematic literature review. ACM Trans Auton Adapt Syst Aug. 2021;15(3):9:1–9:37. https://doi.org/10.1145/3469440.
[34] Scheinker A. Adaptive machine learning for robust diagnostics and control of time-varying particle accelerator components and beams. Information Apr. 2021;12(4). https://doi.org/10.3390/info12040161. Art. no. 4.
[35] Wu Z, Rincon D, Christofides PD. Real-time adaptive machine-learning-based predictive control of nonlinear processes. Ind Eng Chem Res Feb. 2020;59(6):2275–90. https://doi.org/10.1021/acs.iecr.9b03055.
[36] Wong Pak-Kin, Huang Wei, Vong Chi-Man, Yang Zhi-Xin. Adaptive neural tracking control for automotive engine idle speed regulation using extreme learning machine. Neural Comput Appl 2020:32. https://doi.org/10.1007/s00521-019-04482-5.
[37] Millo F, et al. Synergetic application of Zero-, One-, and three-dimensional computational fluid dynamics approaches for hydrogen-fuelled spark ignition engine simulation. SAE Int J Engines Dec. 2021;15(4):561–80. https://doi.org/10.4271/03-15-04-0030.
[38] Brancaleoni PP, et al. Performance evaluation of hydrogen-powered internal combustion engine city bus for the urban mobility of Bologna, Italy. J Phys Conf Ser Nov. 2024;2893(1):012068. https://doi.org/10.1088/1742-6596/2893/1/012068.
[39] Heywood JB. Internal combustion engine fundamentals'. New York, NY: McGraw-Hill; 1988. ISBN: 9780070286375.
[40] Chen SK, Flynn PF. Development of a single cylinder compression ignition research engine. SAE Technical Paper Series 1965. https://doi.org/10.4271/650733.
[41] Qian N. On the momentum term in gradient descent learning algorithms. Neural Netw Jan. 1999;12(1):145–51. https://doi.org/10.1016/S0893-6080(98)00116-6.
[42] cRIO-9030 - NI [Online]. Available: https://www.ni.com/it-it/shop/model/crio-9030.html. [Accessed 27 October 2025].